Technion Aerial Systems 2017
Development of an Autonomous Unmanned Aerial System for AUVSI SUAS Competition

A. Toporek, S. Bajayo, J. Benchetrit, E. Bensoussan, H. Brod, J. Bruner, S. Greenberg, D. Joseph, A. Shender, M. Solovey, I. Tzror, D. Artzi, Y. Gutnik
Faculty of Aerospace Engineering, The Technion, Haifa, 3200003, Israel

D. Ben-David, E. Genius, A. Hasson, N. Ibn-Danan, O. Markus, O. Milul, R. Yehudai, J. Erez
Faculty of Electrical Engineering, The Technion, Haifa, 3200003, Israel

This technical design paper is a summary of the work conducted by the Technion Aerial Systems (TAS) team for the AUVSI Student UAS Competition 2017. The document describes the design of the STRIX system, the rationale behind the design choices, the development process, and the testing performed to enable STRIX to accomplish all its tasks. STRIX is an airplane with a wing-fuselage configuration, equipped with two electricity-powered engines and an all-composite structure. It is capable of autonomous flight, including take-off and landing; its on-board computers enable image processing; it uses "sense and avoid" algorithms that operate online and can calculate routes while still on the ground. The customized user interface (UI) assists in effective control over the system. The design team comprises undergraduate students from the faculties of Aerospace Engineering and Electrical Engineering. This year, the project focused on further improving the system, giving it broader and more reliable capabilities.

I. Introduction

The TAS team set out to develop an autonomous aerial system for ISR missions with the intention of participating in the Association for Unmanned Vehicle Systems International (AUVSI) 2017 SUAS (Student UAS) competition.

With its 15th annual SUAS competition, the AUVSI organization challenges student teams from all around the world in designing, manufacturing and testing fully autonomous systems with capabilities fitting the Concept of Operations, broken into ten tasks. Two full UAVs were constructed, designed to participate in the competition, both fully equipped with all components and sub-systems.

Figure 1. TAS Team

Preprint submitted to 58th Israel Annual Conference on Aerospace Sciences.
Received October 7, 2017.

II. System Engineering Approach

A. Analysis of Mission Requirements

To ensure STRIX meets the performance requirements, we began by performing a thorough analysis of the new competition rules. Using the system entered into the previous year's competition as an example, we focused on analyzing its performance in accordance with the judge's feedback, and explored the changes necessary for excellence under the current year's competition rules. The requirements for the new platform and its flight performance were developed from this analysis.

We used the proven "Red Team" approach to examine the system from top to bottom, in order to gather crucial performance data. With this approach, every team member performs a complete investigation of the project aspects for which he is responsible, and presents the innovations or improvements to be implemented for greater efficiency throughout the system. These areas include aerodynamics, structural design and analysis, propulsion systems, performance of specific competition tasks, interoperability, system integration, etc. The results were first presented at the Technion during the Preliminary Design Review (PDR); the final design was presented at the Critical Design Review (CDR) several weeks later. After the design was set, the work on the new model began.

B. Design Rationale

The decisions made regarding the platform design addressed a number of environmental factors:

- **Team qualifications** – The design should be based to the maximum scale on the team's qualifications and knowledge. This implies evaluation of the team's capabilities in designing all aspects of the system.
- **Time management** – Since time is of the essence, the project design must be feasible in the scope of the time that is available. A reverse timetable was created, with the critical milestones defined by the competition rules (FRR, proof of flight, etc.) and the team's defined schedule.
- **Manufacturing process** – The final solution should suit the team's manufacturing capabilities.
- **Maintainability –** The system should be easy and intuitive to maintain in order to minimize the preparation time between flights and increase the system's reliability.
- **Safety –** The system should guarantee minimum risk, for both the crew operating it and for the system itself. This requirement should drive the creation of hardware safety interlocks and operation checklists.
- **Budget distribution** – Every design choice includes criteria for the financial investment required for its realization. This is sometimes a dominant factor; the budget was therefore distributed in accordance with the task priorities.

The system is required to perform all the competition tasks with excellence. We therefore put our efforts into areas that were not yet realized in the previous years. Our priorities were determined according to the following requirements:

- **Flight endurance and performance** – An aircraft should be able to use the entire defined flight time. A fixed-wing aircraft capable of carrying all the necessary equipment onboard was chosen for the task, in accordance with the payload requirements. An aircraft should be able to reach the minimum turn rate, the highest climb rate, and maintain the defined cruising speed in the search area (this is influenced by the camera shutter speed). These performance parameters have the greatest impact on the aerodynamics requirements, on the propulsion system, and the structural design of the platform requirements.

- **Aerodynamics** – An aircraft must be aerodynamically stable and capable of performing all the required maneuvers, including safe takeoff and landing.
- **Aerodynamic loads –** Design of the airframe structure, which will withstand all the maximal loads, stresses, vibrations, and landing impact applied during the mission.
- **Imaging system** – The camera must meet the mission requirements. Parameters include the resolution, quality, frequency of the images taken, weight, compatibility to the system and reliability.
- **Subsystem compatibility –** Various components must be compatible with each other, to transmit the data and the correct orders. The choice of inner components was affected by this factor.
- **Ground stations –** The stations manned by the human personnel who operate the system from the ground must be reliable, possess high computational capabilities, and be portable. In addition, it must be possible to deploy and operate them quickly and easily.
- **Image Processing** – The appropriate hardware and software must be installed so that the system can perform tasks such as objects detection, localization, and mapping.

This year, we emphasized areas that were not yet realized in the previous platforms. The main concept has undergone numerous improvements:

- **Autonomous landing –** The system can land autonomously. Several design changes were implemented to achieve this task: new wing flaps allow decreasing the touch-down speed, and a range-finder enables more accurate estimation of flight altitude.
- **Obstacle Avoidance Task –** A completely new algorithm was implemented. This sample-based algorithm performs avoidance of static and dynamic obstacles.
- **Propulsion system –** More powerful engine models provide better performance during the flight. The model includes increased propeller diameter and a new engine location to improve aerodynamics, thrust efficiency, and the stability of the system.
- **Airdrop –** A shock absorber was designed and added to the bottle in order to assure safe water delivery.
- **Structure optimization –** The updated composite skin structure decreases the weight of the airplane, increasing flight durability and aerodynamic characteristics. New servos models also contribute to decreasing the platform's overall weight.
- **System installation optimization –** Subsystems were transformed into modular subsystem clusters, in order to ease maintenance overhead.
- **System redundancy improvement –** New, more capable batteries were chosen for the platform. Together with replaced voltage regulators and connectors, they provide improved system capabilities and reliability.
- **Gimbal design –** A new gimbal was designed, offering more accurate stabilization and tracking, as well as a reduction in overall weight.
- **Antenna tracker** – The antenna tracker was renovated and redesigned.
- **Imaging Console –** The imaging console has undergone several improvements, including: better communication with the judges' server and the Mission Planner environment; increased image download speed; improvement of the ADLC

algorithm; increased mapping precision; and Real Time Kinematic (RTK) integration for improved navigation and mapping precision.

C. Programmatic Risks and Mitigation

This year, risk assessment was based on the accumulated experience of previous years and current environmental factors. This section sums up all the evaluations, their probable impacts on the project, and the means by which issues were mitigated, from the most harmful to the least harmful. The risks may be divided into following:

- **Timetable delays**
  If the defined tasks are not completed on time, subsequent tasks are at risk of inheriting the delay; consequently, the entire project may be delayed.
  Mitigation methods:
  - A firm timetable and plans were defined at the beginning of the project. Adherence to this schedule was emphasized as a criterion for the success of the project.
  - Weekly meetings are conducted in order to keep track of the progress of each task and to evaluate the likelihood it will be completed according to the timetable. Some tasks may be performed simultaneously, and others consecutively, thus requiring prioritization.
- **Insufficient mission experience**
  Flight time must be accrued for successful demonstration of the mission.
  Mitigation methods:
  - Flight training for the crew was initiated during the early stages, using last year's design. The complete set of mission capabilities was tested with the old platform, which provided an overall view of the required working process.
  - Mission simulations were performed in order to train pilots using the Software in the Loop (SITL) system.
- **Integration**
  The project brings together a large number of participants from two faculties – Aerospace Engineering and Electrical Engineering. Contradictory engineering requirements or solutions may endanger the operability of the system as a whole. Many solutions require consultation among several project members.
  Mitigation methods:
  - Weekly meetings are conducted as mentioned above. The project team discusses the work of each project member during the meetings.
  - A single supervisor and mentor, highly experienced with leading projects of this scope, to assist in guiding the crew in the development and testing phases, and with organizational aspects.
- **Adherence to the competition rules**
  While maintaining enthusiasm for creating a better airplane, strict adherence to the competition rules is important in order to avoid penalties.
  Mitigation methods:
  - A team member was assigned the task of familiarizing himself with the competition rules at the highest level, so that he could supervise the entire process to ensure the final design met all the requirements.
- **Crash of the airplane**
  As in any system, there is a risk of failure during the real-time mission. If this happens during the final demonstration, not much can be done; however, the effects of a crash during the preceding flights can be mitigated.

Mitigation methods:

- Some of the training missions were conducted on the previous year's system and Test Model A/C.
- Two additional vehicles were constructed to serve as a backup in case of accident.

III. System Design

This section describes the design of the UAS system. It covers all areas of platform development, the design rationale for implementing each decision, and the selection of the final design solutions.

D. Aircraft

This section describes the design of the aircraft, including its build, the aerodynamics and propulsion aspects, the payload system, and the general architecture. The improvements made to the system in the current year are emphasized.

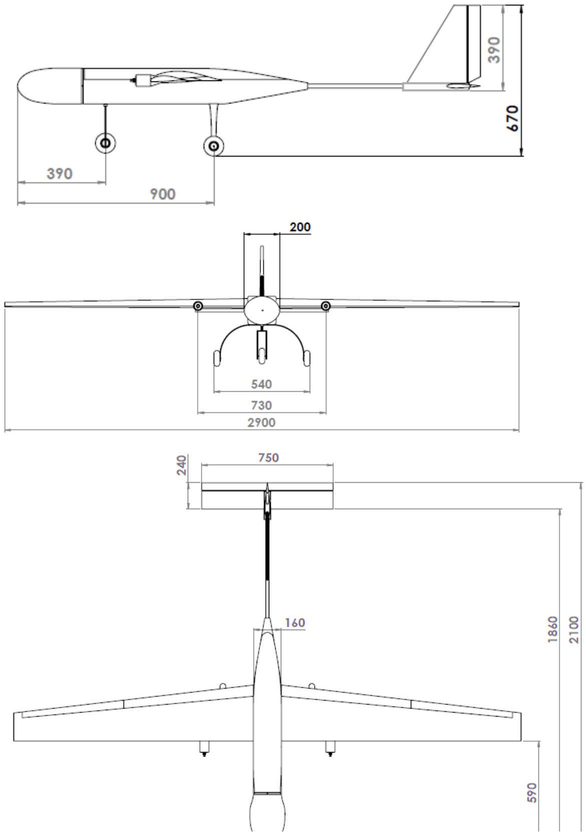

Figure 2. STRIX system drawings: Left, Front, Top

1. Design

The 2017 aircraft structure comprises five parts: two wings, the fuselage, the tail unit, and the upper access panel. Each part is designed to be detachable in order to allow quick access to all the inner airplane subsystems, easy maintenance, and convenient transportation. Figure 2 illustrates the general outer structure and provides the dimensions of the airplane.

Although the configuration is similar to that of the previous year, several major changes were implemented to improve system performance during missions. The structure was optimized by reducing the platform's weight, while maintaining the structural strength in the flight envelope.

The wing structure is hollow, comprised of a "sandwich" of two skin layers, with a "U" section beam. The main beam is designed to support the bending stresses of the wing. The aft beam, the main beam, and the skins define the torsion box of the wing.

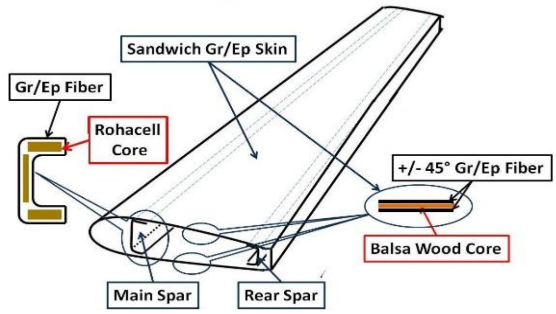

Figure 3. Hollow All-Composite Wing

Since one of the biggest surfaces of the airframe is the wing's skin, we focused on its optimization. It was decided to retain the sandwich structure of the carbon–balsa wood core, and reduce weight by changing the thickness and stiffness of the balsa core while keeping the same carbon layers. In order to choose the optimal mechanical properties of the wing skin, two tests were conducted: a strain experiment and a 3-point bending experiment. The weight of each sample was also compared.

In addition, finite element analysis was performed in order to determine stress along the wing span and wing tip deflection. Finally, we performed a wing loading experiment to validate the theoretical estimates and the manufacturing process. The results may be seen in the appropriating section in the document. In addition, along the fuselage itself, four imbedded longerones were installed between the layers to further increase the bending stiffness. Several frames and reinforcements were added in places of concentrated loads.

In order to further reduce its weight, we chose to use a 120 g/m^2 carbon fiber woven sheet, instead of the previously used 195 g/m^2 carbon fiber sheet. In addition, we reduced the number of layers that were used, keeping in mind the overall desired airframe strength.

The aft portion of the fuselage comprises a detachable cylindrical tube made of a unidirectional carbon layer on top of a plain weave layer with an epoxy polymer composite. This resulted in a further reduction in weight, compared to the previous year. Figures 4 and 5 provide a general overview of the airplane, with the inner systems installed.

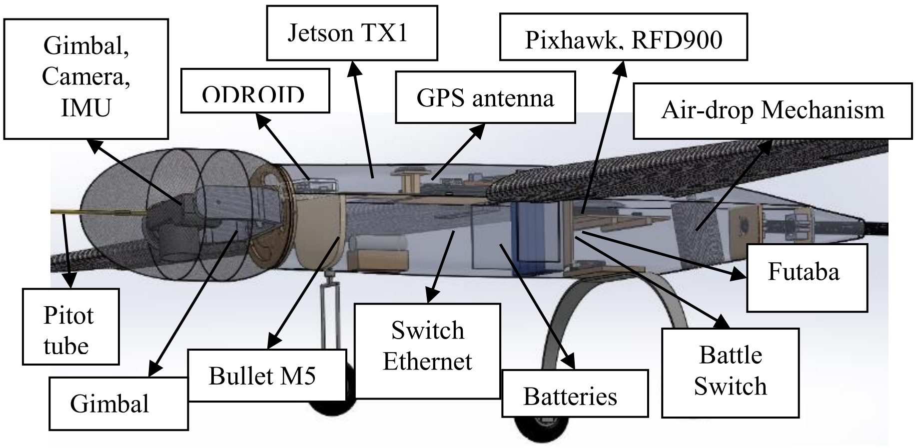

Figure 4. STRIX overview, main components labeled

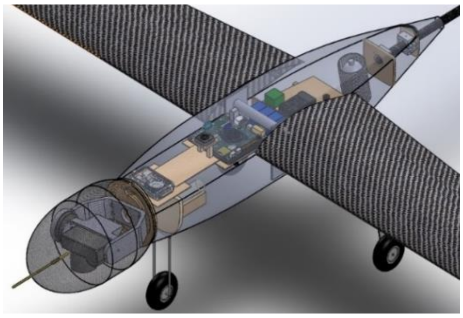

Figure 5. Airplane overview

Table1. STRIX characteristics

Main Wing		Vertical Stabilizer		Horizontal Stabilizer		Aircraft Dimensions	
Airfoil	Douglas LA203A	Airfoil	NACA 0012	Airfoil	NACA 0012	Length	2.09 m
Span	2.9 m	Span	0.35 m	Span	0.75 m	Width	2.9 m
Area	0.708 m^2	Area	0.085 m^2	Area	0.165 m^2	Height	0.686 m
Aspect ratio	11.85	Aspect ratio	1.44	Aspect ratio	3.4	Weight	12 Kg
Figures of merit		**Propulsion System**		**Velocity**		**Endurance**	35 min
Wing loading	16.9 kg/m^2	Motor power	2700 W	Stall speed	23 knots	Range	18.6 nmi
Power loading	225 W/kg	Prop. size	18X10	Cruise speed	32 knots	Rate of climb	600 ft/min
Max load factor	3.5	Batteries	14.8 V 30 Ah	Max speed	50 knots	Minimal turn radius	60 ft

Preprint submitted to 58th Israel Annual Conference on Aerospace Sciences.
Received October 7, 2017.

2. Aerodynamics

During the current year, the main emphasis in aerodynamics was put into four main improvements: engine location optimization, tail stabilizer redesign, the addition of wing flaps, and a new, aerodynamic gimbal cover design.

- <u>Engine Location:</u>

In the red team examination, we found that no attention was given to the location of the engines in the previous year's project. As the engines are located on the wings, they have a great deal of influence on the air flow around the wings. It was decided to look into the location of the engines more closely. Engine location influences several aspects, such as air flow around the wings, blade clearance from the fuselage and the ground, stability in the event an engine loses power, and ease of manufacturing. In addition, there are several parameters that define the location of the engines, which include the spanwise location (distance from the center line), the vertical location (distance from the cord upward or downward), the mounting angle (angle between the engine axis and the chord), rotation direction, and the streamwise location.

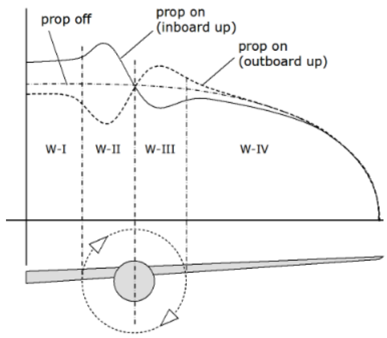

Figure 6. Lift distribution dependence on direction of propeller rotation

Due to limitations in the manufacturing capabilities, it was decided to retain the mounting angle of 0 degrees, the vertical location to be at the chord, and the same streamwise location of the same position as in the previous year, although all those parameters do affect the local angle of attack. On the contrary, the rotation and the spanwise location, which also affect the local angle of attack, have no effect on the complexity of manufacturing.

The wing closer to the airplane fuselage has a longer chord, which contributes more to the lift; it was therefore decided to rotate the propellers inboard up, as described in Figure 6. While the spanwise location has a negligible effect, there is still an increase in performance proportional to the distance of the engines from the center line. The more important aspects are the ground clearance and the lateral stability in the event a single engine is lost. In analyzing the ground clearance for landing on one wheel, it was found that for the STRIX propellers of 18 inches, the location of the engines is required to be at most 460 mm from the centerline.

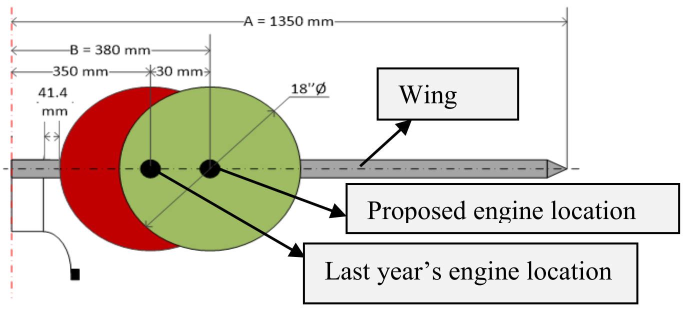

Figure 7. Engine location repositioning

Lateral stability in the event of engine loss must also be considered. In this situation, the single engine is required to overcome the drag forces, and in general, provide additional thrust in the event of emergency. While performing these maneuvers, lateral airplane stability must be maintained.

The thrust the single engine must provide in this case must be at least the value of last year's design. In that extreme case, it was verified that the vertical stabilizer provides a sufficient countering moment at the maximum sliding angle, which is proved in the following table. The forces in the calculations are pictured on the right side of the table.

Table 2. Tail and engine moment

	arm [m]	force [N]	force [kgf]	moment [Nm]
Tail moment	1.16	7.29	0.74	8.43
Engine moment	0.38	22.18	2.26	8.43

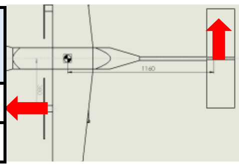

By comparing the existing twin-engine configuration planes, we can observe that the average engine location/half-wing (A/B in Figure 7) span is 0.275.
If we consider the ratio to be the average of the presented airplanes, the engines in our system must be located 371 mm from the center line. In the STRIX design, the engines are located 380 mm outboard from the centerline, staying relatively close to the recommended value. From this, we will put a limit on engine thrust for single engine loss to 2.2 kgf.

- <u>Vertical Stabilizer:</u>
  This year, we improved the aerodynamics and structure of the vertical stabilizer by eliminating the dorsal fin. We incorporated its stabilization moment into a new integral shape of the vertical stabilizer, which was evaluated and tested during the flight tests.
  We found that the new tail increased the tail volume by about 300 cm^3, 0.3 %. While the moment remains almost the same, the wetted area decreases by 91 cm^2, 9.6 %, meaning less drag for the new design of the tail stabilizer.

Figure 8. Vertical stabilizer redesign

- <u>Wing Flaps:</u>
  The main improvements include the wing configuration. Flaps were added to the wings to enable autonomous landing and minimize the risk of high speed touchdown impact. It was decided to add a 0.25 chord plain flap along the existing aileron line. According to our analysis, the addition of flaps will increase the maximum lift coefficient during landing by 0.6 and decrease stall speed by 15%. Consequently, it will decrease the touchdown speed. These benefits will help us to perform soft, safe autonomous landings, minimize the risks involved in that action, and increase our system reliability. The addition of flaps is a low-cost solution which is simple to produce.

Preprint submitted to 58th Israel Annual Conference on Aerospace Sciences.
Received October 7, 2017.

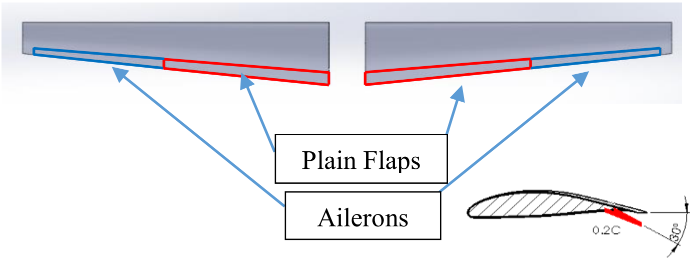

Figure 9. Wing flap addition overview

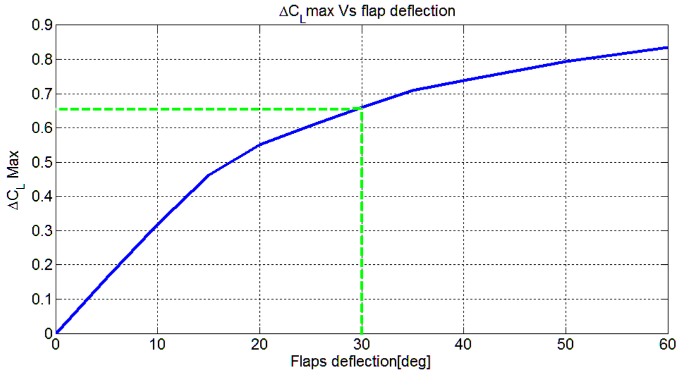

Figure 10. Increase in Cl parameter vs the flap angle

- Nose Cover:
  The gimbal shell shape was redesigned in order to reduce the aircraft drag and improve its lateral stability. The nose was adapted to have the same height as the fuselage of the aircraft and the cross-section of the nose was reduced to the minimum. Its dimensions were chosen to accommodate the gimbal and camera with minimum required clearance. Figure 11 illustrates the entire new gimbal and nose.

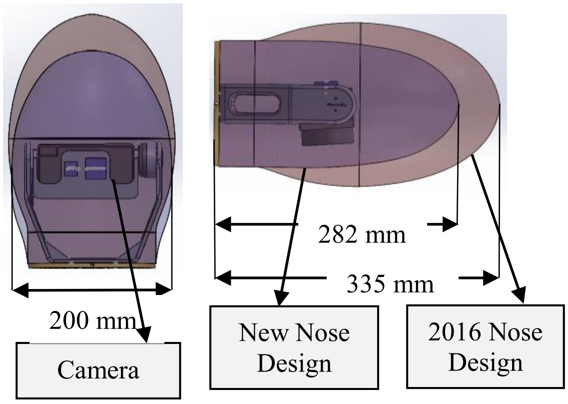

Figure 11. Nose cover redesign

3. *Fabrication*

First, the molds for the aircraft parts were designed using a 3D CAD model. The mold was produced from MDF wood, using CNC machinery. A total of 50–52 epoxy-infused composite layers were then placed onto the mold and vacuum bagged. Once the epoxy-infused carbon composite hardened, the part was then trimmed to the correct dimensions and shape. In addition, 3M DP460 structural epoxy adhesive was used as needed.

The fuselage consists of carbon/epoxy layers (with a specific weight of 195 g/m). The open "U" cross section of the fuselage was reinforced by four embedded reinforcements made of unidirectional (UD) graphite and a Rohacell core, to increase the fuselage's bending resistance.

Additional reinforcement ribs were added to critically stressed spots.

The aileron/flap hinges were made of Aramid fiber (Kevlar), and were integrated inside the layered structure of the upper wing skin. The wings were connected to the fuselage using a carbon tube, which was inserted into the aluminum housing within each wing. The wing joiner was inserted into the wing–fuselage attachment on the fuselage.

Figure 12. Fuselage fabrication

Preprint submitted to 58th Israel Annual Conference on Aerospace Sciences.
Received October 7, 2017.

4. Propulsion

This year's UAV is maintaining the twin motor configuration of the previous year's platforms, retaining one motor on each wing. This twin motor configuration is suitable to our fail-safe design, to achieve safe landing in the event one of the motors fails during the flight. In addition, this configuration allows us to use a front payload mechanism (a gimbaled high resolution camera) without any disturbance by landing gear or propellers.

After evaluating last year's flights and a crash of one of our platforms during a touch & go maneuver, the cause of the crash was investigated. Taking into account the increased weight of the platform, the investigation concluded that the propulsion system provides an insufficient thrust-to-weight ratio (T/W). We therefore decided to employ a new combination of motors, electronic speed control (ESC), and propellers to resolve the problem.

In order to find the right configuration for us a research of new motors and ESC was preformed, since propeller size is limited due to the height of the airframe and a minimum clear distance from ground was required we choose to increase the propeller diameter to 18" while leaving the pitch between 9 to 12 depending on the motors rpm.

The new combination was chosen to increase the T/W ratio to the maximum, while maintaining adequate flight time to complete the competition tasks.

The final configuration is: 2X Scorpion HKIII-4035-560 motors, Scorpion Tribunus 120A ESC, and APC 18X12 propellers. The (T/W) ratio increase in comparison to the last year's design is 2.3.

The static details above were concluded from static trust tests using a bench test in the workshop.

Batteries were a hard decision since flight time goal was 30 min our old battery configuration provided us with 26 Ah capacity giving us around 28 min flight time with optimal new batteries. Although this year's propulsion is more than twice as powerful as the previous one, this system is much more energy-efficient due to the quality of internal components better wiring design by the team and less connectors.

After a lot of debates around adding an extra battery of changing battery capacity we decided to increase each battery capacity to 10Ah using tree of their batteries we get a total capacity of 30Ah (4000mAh more than 5X 5.2Ah batteries) this change provided us with approximately 30 min of flight time.

In order to be on the safe side we decided to add a fourth battery, even though we ended up with a 400 gram increase in power bank weight we achieved to get above 45 min flight time.

5. General Architecture

This year, for the STRIX, we decided to make a significant change to the architecture of the Athena last year platform. The architecture is very complex for a little platform like ours and it was our main objective to improve it and make it a lot easier to maintain.

Many systems, sensors and computers need to communicate with each other for the plane to fly autonomously and accomplish the requested missions. Moreover, there are four different power suppliers, and in case of a malfunction of one of them, we need to have a backup for the safety pilot so he can land the plane safely. We looked into the possibility of reducing the number of power suppliers and get to the conclusion that it's only possible if we change existing components, like the camera for example, but the time didn't allow us to do so.

We presented our solution for this year: split the architecture in two main compartments: the control system and the payload system. The control system includes all the components required for the autonomous flight (except the pitot tube which need to be in front of the plane) and is located at the back of the STRIX. The payload system includes all the components required for the imagery system and communication with the ground station through the bullet M5. Every compartment contains the power suppliers he needs so that in case of a payload dysfunction, it does not interfere with the control system and we can save the plane.

After that, we needed to review the wiring system of last year. Most of the issues are coming from an unstable and fragile wiring. The number of wires required for the entire plane made us think of a new solution: the use of large connector to minimize the wires next to the batteries and the risk of disconnections between the components. The connectors improve also the understanding and the handling of the system. Less wires and more order into the structure of the plane reduce weight and it's one of our primary objectives.

Conclusion: maintenance is easier in this year STRIX, the system is more reliable, replacement of a bad component is easier and transfer for one plane to another is easier. A better architecture and system integration for a better plane.

Figure 13 illustrates the general architecture of the system, showing all the internal subsystems and components. Table 3 shows the contents of each system module.

Table 3. Module architecture

Payload System Module	Control System Module
Jetson TK1	Pixhawk PX4
Gimbal Controller	Futaba R6208SB
Odroid XU3	BattleSwitch
Bullet M5	RFD 900
Ethernet switch	S-Bus

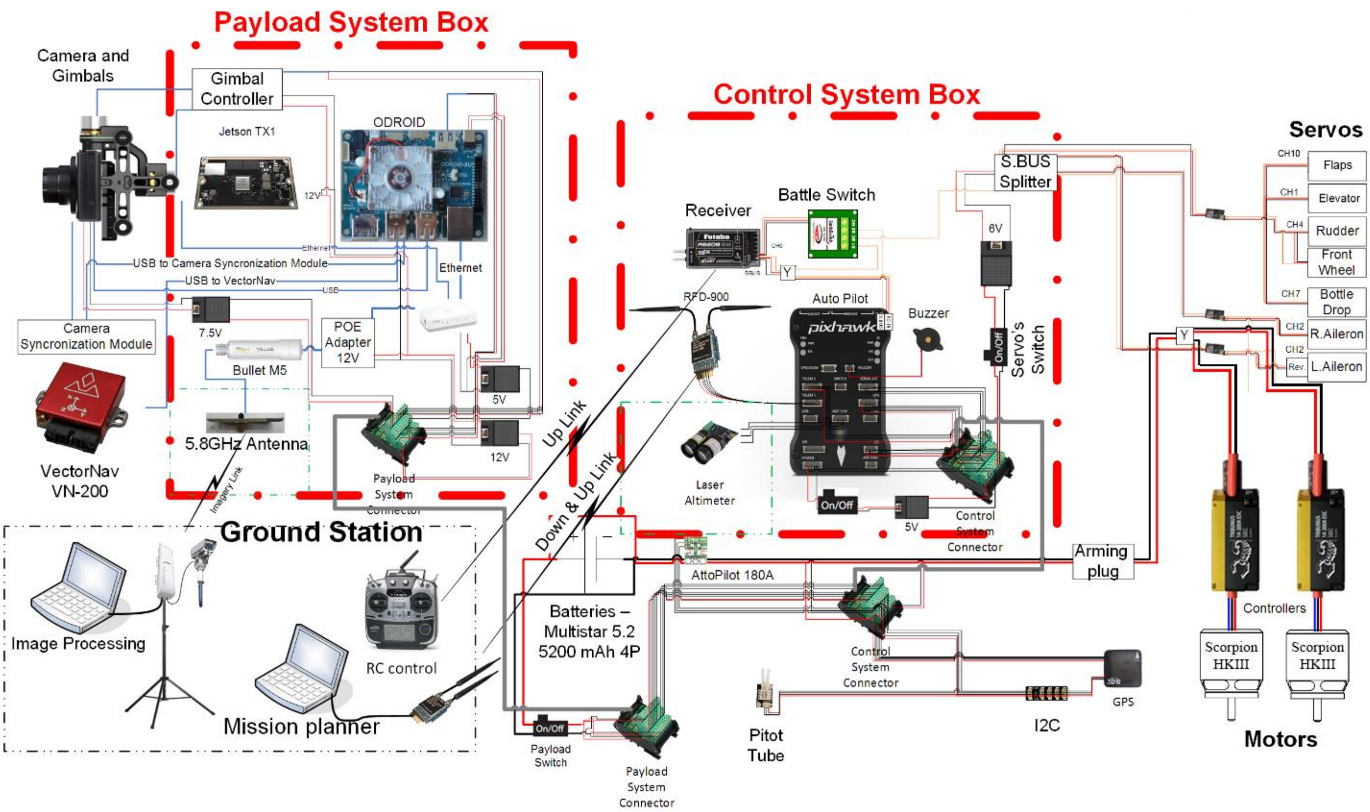

Figure 13. STRIX System Architecture

6. Payload – Gimbal

One of the most important missions of this project is the target detection. To complete this mission, a good camera with excellent accuracy is required, this accuracy can be reach by stabilizing the camera. The best way to stabilize a camera in an unnamed aircraft is to use a gimbal. In our project, because of the maneuvering of the plane, a two-axis gimbal system has been used, based on rotation about the pitch and roll axes.

In order to reach the goal of reducing the total airplane weight, as we decided to do at the beginning of this project, the gimbal weight had to be reduced compared to its previous configuration. The challenge in this case is to build a strong gimbal which will not break under the different forces applied during the flight and maneuvering, while minimizing the gimbal's weight so as not to affect the aircraft's center of mass, thus not changing the fuselage dimensions.

An optimization of the gimbal's design has been performed by mechanical design work. Some weight reducing holes have been added, and all the gimbal dimensions reduced. The use of a stronger material: ABS with a density of 1.04 g/cc and a Tensile Strength of 43 MPa, will ensure that the modifications will not affect the gimbal's strength.

After the redesign, a strength Analysis is required to make sure that the gimbal will not fail during flight (SolidWorks application was used to perform this analysis). The maximum force caused by the camera was evaluated to be about 17.2 N: the mass of the camera is 0.5 kg, multiply by g(=9.81) multiply by 3.5. Another important aspect of the gimbal is the inclusion of two separate axis motors. Two brushless motors were chosen: one with a torque of 2200 g @ 5 V and 0.6 A for the roll axis, and another with a torque of 700 g @ 5 V and 0.43 A for the pitch axis.

Based on the analysis, it can be evaluated that the maximum stress in the gimbal structure is about 9.5 MPa which is significantly below the maximum material strength. This analysis proved that the new, mechanical design will work appropriately.

Another important aspect of the gimbal is its motion about the pitch and roll axes. To ensure fulfilling these motion demands, the inclusion of two separate axis motors was necessary. After searching the adapted motors which can rotate the gimbal with the camera, two brushless motors have been chosen: one with a torque of 2200g @ 5V & 0.6A for the roll axis and another with a torque of 700g @ 5V & 0.43A for the pitch axis (Fig 15).

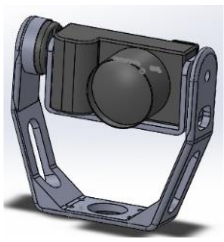

Figure 14. Gimbal

Figure 15. Brushless Motors

After redesigning the gimbal, the aircraft nose had to be redesigned also, the principal goals being: reducing drag and improving lateral stability. To perform these goals, the nose was adapted to have the same height as the body of the aircraft. Consequently, the cross section of the nose was significantly reduced when compared to the old design as shown in Fig 16. It must be said that the Pitot tube installation which is located in the front of the nose was not affected by the design change, and it remained in the same place.

In conclusion, the two goals dictated at the beginning of the project were to reach a minimum cross-section of the nose to improve the lateral stability of the aircraft, and to reduce the gimbal weight in order to reduce the total aircraft weight. This was accomplished by redesigning the gimbal, changing its material manufacturing, and improving the axis

Preprint submitted to 58th Israel Annual Conference on Aerospace Sciences.
Received October 7, 2017.

motors. The nose of the aircraft was adapted to the new gimbal, and reduced by 25%. An illustration of the entire new gimbal with the new nose at the aircraft is shown in Fig 5 and Fig 6.

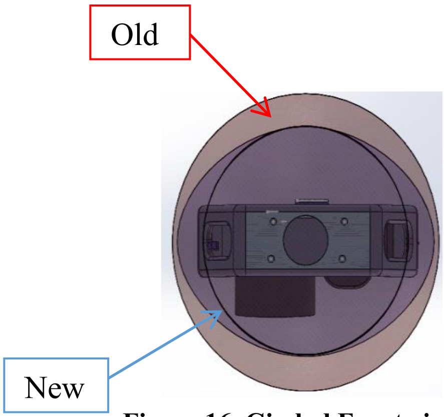

Figure 16. Gimbal Front view

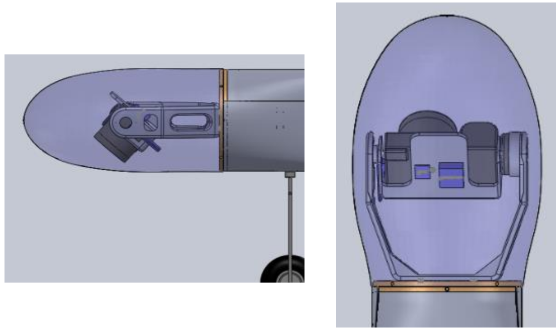

Figure 17. Gimbal Side and Top view

- <u>Gimbal Motion Controller:</u>
  The gimbal motion controller was selected to be - STORM32 controller. STORM32 is a relatively low-cost 3- axis brushless gimbal controller that communicate via MAVLink protocol on board.
  The STORM32 has a built-in Pixhawk support and separate PID controllers for each rotation axis. By attaching an IMU module to the camera's horizontal plane it was possible to ensure an outstanding orientation control of the camera.

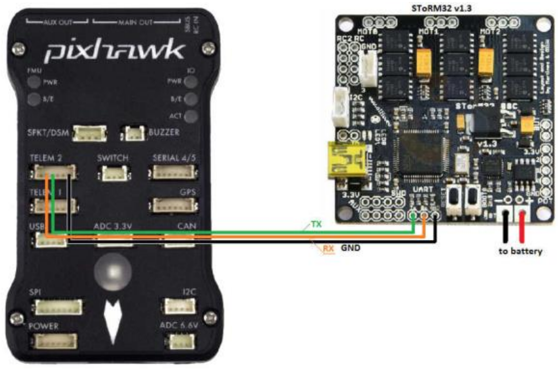

Figure 18. Gimbal controller connection to Pixhawk

- <u>Gimbal Controller – UI:</u>
  Storm32 controller support a friendly UI (User Interface)for configuration. With the user interface it was possible to load firmware, configure motors properties, tune the PID Parameters, adjust motors Voltage , rotating speed and angles limitations.
  It was also possible to see IMU's status and orientations during operation on ground.

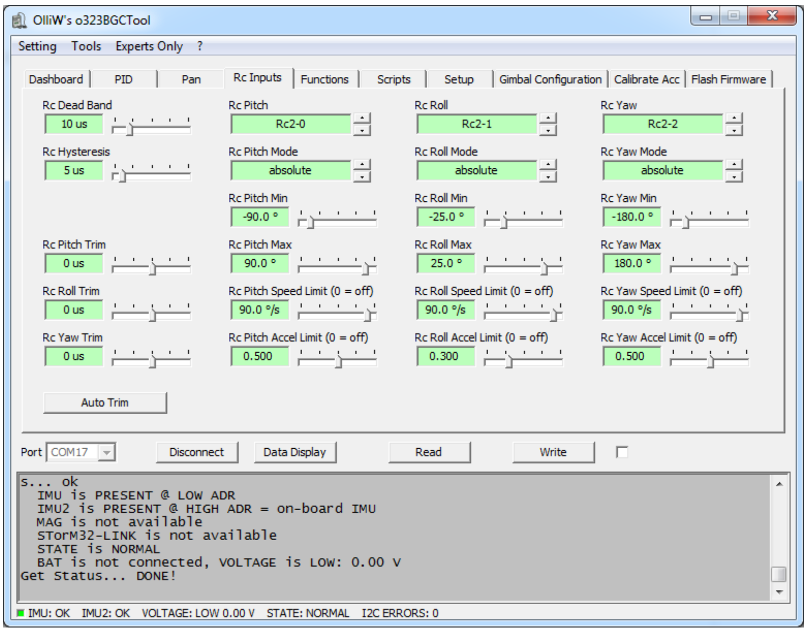

Figure 19. Gimbal parameters tuning

- <u>Gimbal Orientation – Tests and Simulations:</u>
  First step that was performed was to configure the STORM32 controller board to the new motors – number of poles voltage limitations etc. After the controller was adjusted to the motors, a PID tuning procedure was executed in order to achieve a sufficient close loop behavior in each rotating axis.
  We examined gimbal's close loop behavior for a Step input of 45 degrees for roll movement and 25 degrees for pitch movement (typical orientation that needed according to competition's rules). According to gimbal behavior on each axis, PID parameters were tuned until an optimize behavior was achieved.

E. Obstacle Avoidance

In order to successfully complete the Obstacle Avoidance task, we proposed and implemented a new, innovative method. This method belongs to the series of the Sampling-Based Motion Planning algorithms. The STRIX system uses the Rapidly Exploring Random Tree (RRT) algorithm (further on: The Algorithm) as the basis and its extension, called the RRT-star, which aids in finding the most optimal path – a trajectory between the waypoints that minimizes the cost function, subject to given constraints (e.g., obstacles ad flight zone). The function is based on sampling random points in the region of interest (nodes), connecting them in the form of a path net to existing nodes, further investigation of the cost function of reaching every one of them, and rewiring the net in the process of adding the new nodes.

The following is the detailed explanation of the process.

First, the new node q_{rand} is the generated node with random position. If its distance from the nearest node with the lowest cost function ($q_{nearest}$) is greater than V – largest net branch length defined by the user, The Algorithm moves it in this direction vector until the distance V is achieved (denoted as q_{new}). If no obstacles are encountered in between q_{new} and $q_{nearest}$, the node is being connected to the net. Each node has a parent, and can have several "children".

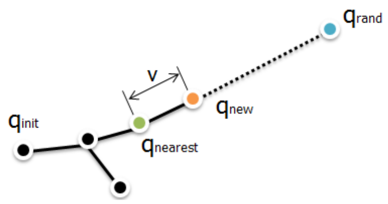

Figure 20. RRT: new node generation

The cost function for every node consists of the cumulative distance through all its parents to the origin node.

The second function, which poses the most significant difference between the RRT and RRT* model, is the "Rewire" function, illustrated in the Fig 21. After the node is being connected to the main net, a search is being performed on the nodes around it, each of those is being analyzed (marked as green, q_{near}). If the cost function of connecting this node to the q_{new} is smaller than their original cost function, the rewire process takes place and the q_{new} becomes its new parent. The cost function is being recalculated to every of its children as well. Figure 22 demonstrates how the tree grows with increasing number of iterations, allowing to find an obstacle-free path to every point in the area.

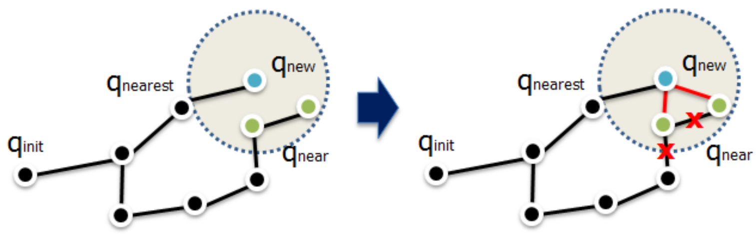

Figure 21. RRT: tree rewiring algorithm

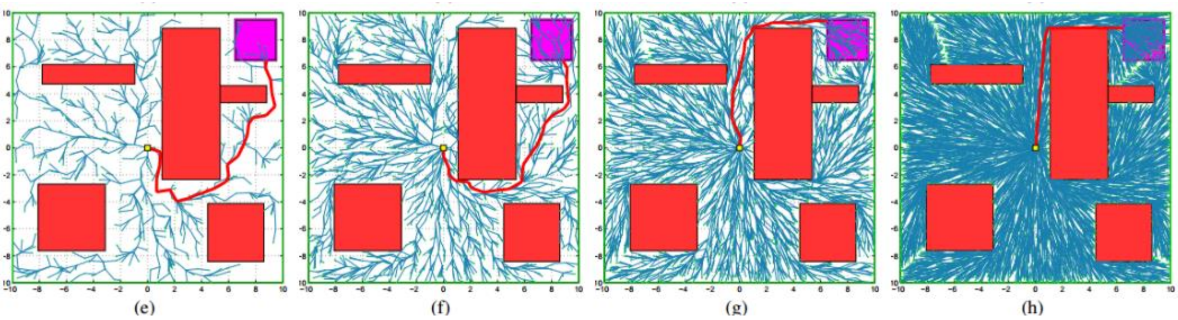

Figure 22. Typical RRT* tree map

The algorithm was first implemented in the MATLAB software, where its performance was analyzed and proven to be feasible and effective. Dedicated graphical user interface (GUI) was developed to make the testing more convenient and user-friendly.

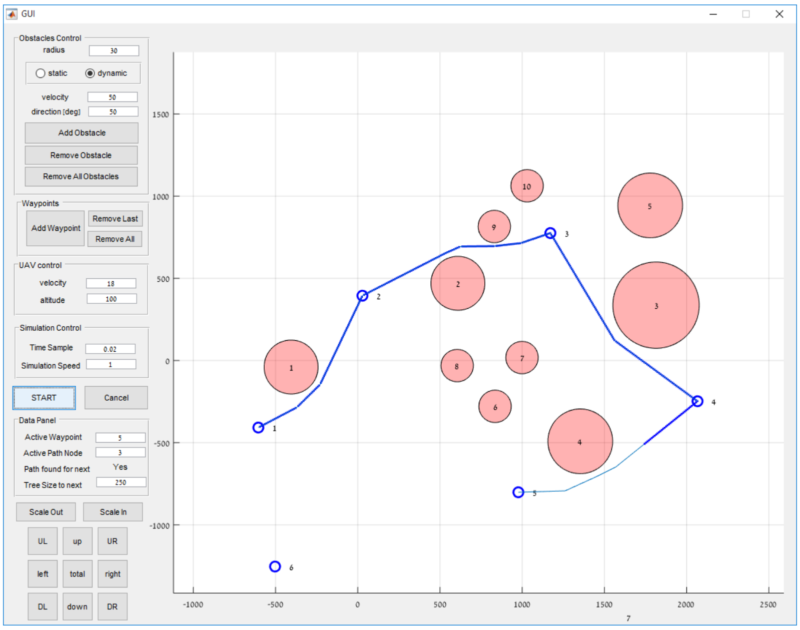

Figure 23. MATLAB RRT* GUI

The process of path calculation can be performed at any time and takes into consideration the waypoints that the platform is about to move along. By examining each sequential pair of waypoints for collision detection (taking the fly-zone borders into consideration), the algorithm is then run on those waypoints in which the detection returns a positive result. Another script is then executed to eliminate the superfluous waypoints in the flight path. The aim is to give a minimal number of commands to the aircraft in order to fulfill the task while ensuring the aircraft's behavior is not overly complex during flight.

It was implemented in the Mission Planner software and is executed now as an integral part of the Mission Planner environment. Figure 23 displays the Mission Planner GUI, where the platform succeeds in finding the path among an array of obstacles and automatically changes the route of the UAV to eliminate any chance of collision, even while the UAV is still on the ground. Last year's algorithm, which operates online, is maintained as the backup solution in the event the main algorithm fails.

The algorithm has been tested in the Mission Planner software numerous times with vast variety of possible waypoints and obstacles locations and parameters using the SITL technique to mimic the behavior of a real RC plane connected to the system. (this technique is explained in the following chapter).

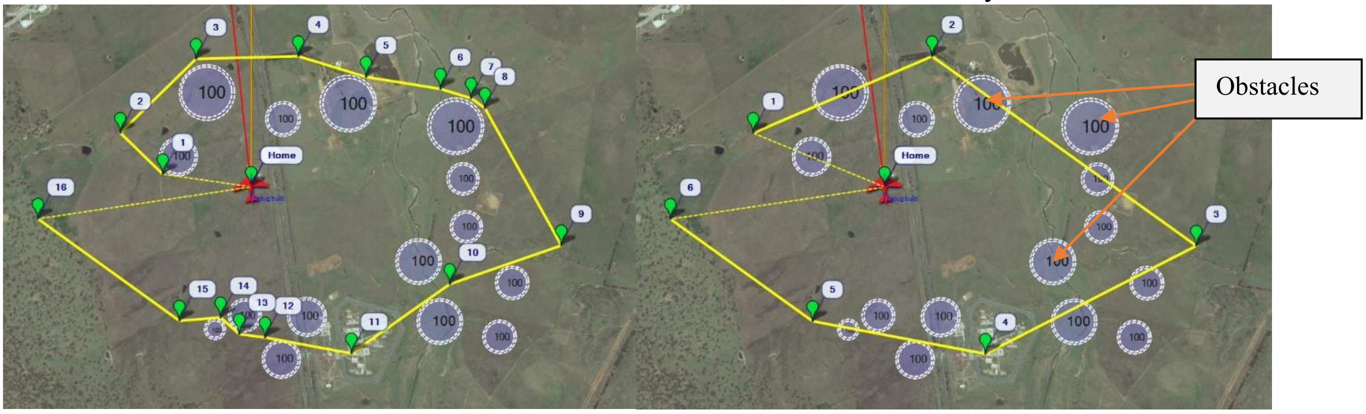

Figure 24. SDA algorithm handling an array of targets (right image – before, left image – after)

F. Simulations Environment

In order to test various features in the software, to debug different algorithms, and to train pilots without any use of hardware connected (Plane, Copter or Rover), the SITL (Software in the Loop) Simulator has been used.

SITL allows the user to run ArduPilot on PC directly. The data of the sensors comes from the flight dynamics model in a flight simulator, in our case chosen to be JSBSim flight simulator. It is knows and a sophisticated flight simulator that is used as the core flight dynamics system for several well-known flight simulation systems. It provides a way to get extremely high frame rate simulation, which is essential for the register level sensor emulation that is used in the SITL build. In addition, it comes as a default flight simulator for ArduPilot, so there was no need to search for a substitute. Below is presented the overview of MAVProxy GCS (Ground Control Station), which is being used by JSBSim.

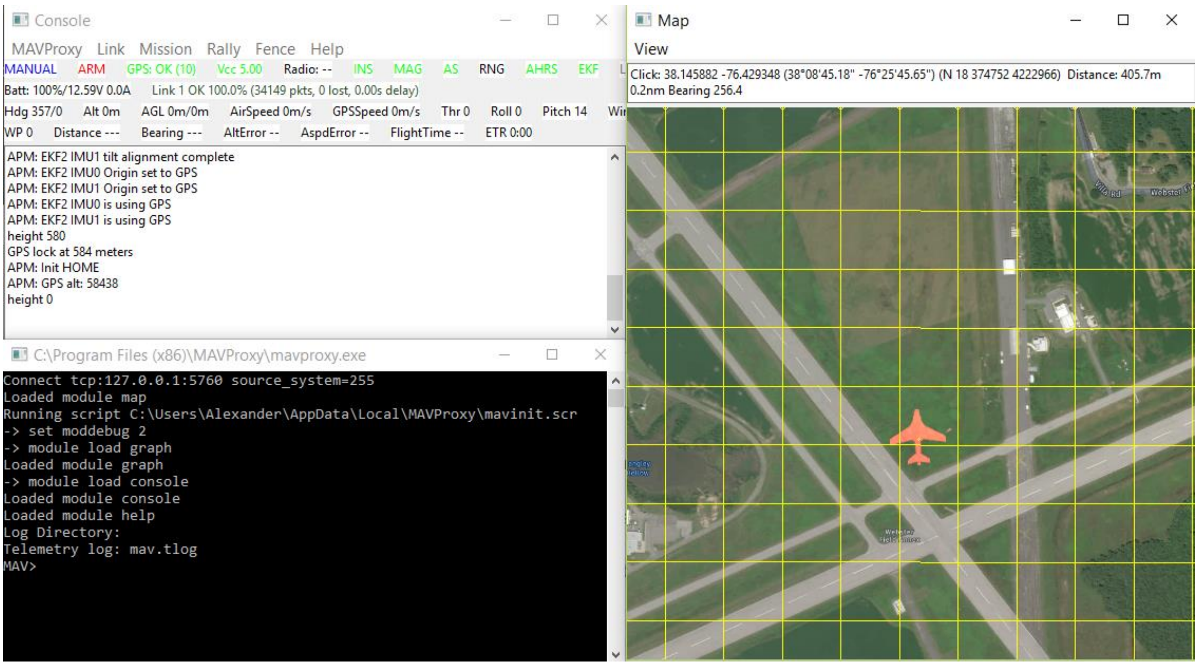

Figure 25. MAVProxy GUI

It has a Console, where all the information and commands may be received through the minimalistic GUI, CMD command line allows to manually control different features. The map displays the Plane location and the environment and can also receive commands such as “Go-To”.

Since we aren't interesting in using this GCS, there is an option to connect to it from the Mission Planner software, which meets our needs much more conveniently. The connection in the Mission Planner to the MAVProxy is performed through the UPD (User Detagram Protocol), through the default local port. Afterwards the Mission Planner will identify the simulated airplane in its environment, which will react to all existing commands with the same behavior as the real UAV connected through the RFD-900 to the Pixhawk. The next Figure displays the complete schema:

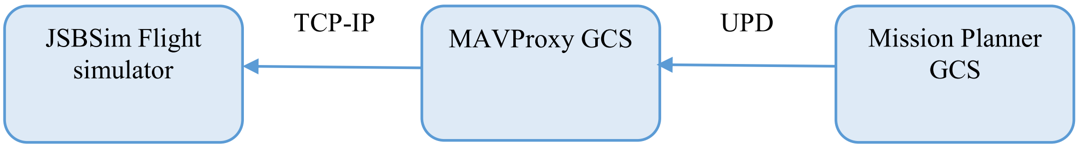

The benefits of using this system may be substantial for the Software Development, Algorithms Development and pilots training. Nevertheless, it should be taken into account that the simulation does not fully represent the real-life scenario. Several of the things neglected / not being accurate are:

- The transmission rate between the GCS and the Pixhawk (connectivity) is much slower in real life, and has several more limitations.
- The model represents a generic RC controlled plane, but many of its parameters might differ from those of our UAV. The flight dynamics cannot fully represent those of STRIX.

G. Imaging System (Payload System)

High resolution pictures and sufficient computing power are required for both manual and automatic target recognition, along with satisfactory frame rate. A separate survey was conducted regarding all parts of the payload, the camera, the gimbal, the interface between the camera to the onboard computers and to the ground station, the efficiency of the onboard computers in terms of computing power, power consumption, physical dimensions, and cost efficiency. The survey showed that there is no need to replace the Sony a6000 camera from last year's system and that newer versions of the camera or other camera type options do not give us significant advantages. It was therefore decided to concentrate on improving the other parts of the payload system.

In short, the Sony a6000 has a 24-megapixel APS-C CMOS sensor and we use it with a Sony 16-50 F3.5-5.6 OSS lens, which provides 3.1x zoom and a focal range of 24–75 mm (35 mm sensor equivalent). The camera is attached to a 2-axis gimbal and is connected to an on-board computer (OBC) via USB cable. Real-time positioning and orientation of the camera is tracked using a dedicated Attitude and Heading Reference System (AHRS). A custom circuit uses the camera's flash signal to achieve precise synchronization between images and the AHRS readings.

In order to improve system stability, the Sony a6000 was equipped with a new metal-oxide semiconductor field-effect transistor (MOSFET) custom circuit to enable hard reset option during flight.

The ODROID OBC, which handles camera control and communication with the imagery console, was updated from version XU3 to XU4. This version has much more computing power, with lower power consumption and smaller dimensions.

The dedicated onboard computer (OBC) that handles image processing tasks was updated from NVIDIA Jetson TK1 to the Jetson TX1 for the same reasons.

This setup ensures quality and reliability of image acquisition and processing and minimizes the risk of performance loss. System wiring was redesigned in accordance with the above modifications. The new wiring scheme provides an excellent tool for health monitoring and ensuring safe operation and testing of the platform.

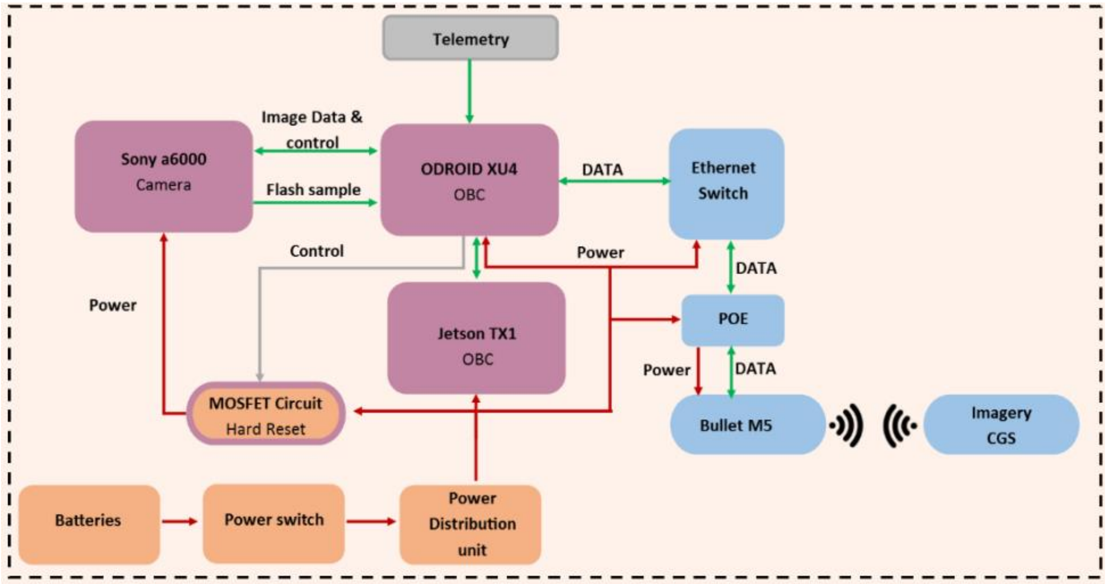

Figure 26. Imaging system architecture

- Camera Abilities:
  In order to accomplish the target recognition task, the camera specifications require inclusion of the following:
  - Ability to change settings during the flight to ensure the best quality under changing environment conditions.
  - High image quality in order to distinguish objects in the photos taken from a high altitude.
  - Satisfactory frame rate for faster SOG.

  Due to the above requirements, it was decided to use the Sony Alpha 6000 camera. In the following section, the camera selection process is described in detail.
- Camera Interface:
  The camera chosen for the mission (due to its optical parameters - Sony Alpha 6000) has only the WIFI adapter available. Its use would result in slow FPS and interference with the FUTABA antenna, thus complicating the RF design. In order to eliminate this issue, a Picture Transfer Protocol (PTP) driver was developed which enables the usage of the USB adapter, thus increasing the rate to 2 FPS.
  Another system synchronizes the captured images with positioning data collected from the GPS, AHRS, and compass, thus significantly improving the accuracy of the target geolocation and mapping algorithms. The timing error using this method does not exceed 10–60 ms due to the data collected last year.

H. Object Detection, Classification, and Localization

Object recognition and characterization can be achieved both manually and autonomously. Below is a review of each of the systems.

- Manual Detection:
  Manual object detection is done using the imaging console (IC). Images are taken automatically and continuously throughout the flight, and thumbnails (reduced images) are sent from the UAV to the IC in order to reduce the bandwidth required per image. Each image is scanned by an operator, which can ask for

cropped, full resolution images of particularly interesting areas. If a cropped image contains a real object, the operator can characterize the object using a GUI developed for this mission. Image location and orientation are automatically calculated by the system, and are integral parts of image characterization.

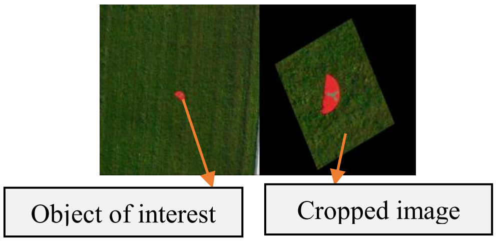

Figure 27. manual detection

- <u>Autonomous Detection:</u>
  The Autonomous Detection, Localization and Classification (ADLC) system is based on state-of-the-art deep-learning algorithms. The system comprises several subsystems, as shown in Fig. 28. The first is called "blob detection" and is responsible for suggesting possible targets (candidates). To do so, it uses the Maximally Stable External Regions (MSER) algorithm. The input of this block is a grayscale, down-sampled image (1600x1080 pixels). A down-scaled image is used due to computational considerations: the MSER is a computational intensive and sequential algorithm, which makes it hard to accelerate using our Jetson TX1 (GPU). The output of this system is a set of 2D coordinates defining blobs. These blobs are fed into the next block – a convolutional neural network (CNN), implemented using the Caffe framework. The purpose of this CNN is to classify the blobs into shapes (circles, rectangles, etc.) and irrelevant blobs (no shape detected).
  The next block is responsible for character classification. For input, it takes patches from full-resolution images classified as containing target shapes. The first stage is character–background segmentation, using a K-means clustering algorithm. The output of this stage is a "character" binary mask. This mask is rotated at 12 different angles. Each mask is resized into a 28x28 pixel image, and is then fed into another CNN (the second stage). The output of the second CNN may be a certain character, or "no-target" tag, for each one of the 12 rotated images. The angle whose character class receives the highest probability is selected as the shape orientation and the corresponding class is used as the shape character. If all the rotated patches are discarded by the network ("no-target" tag), then the patch itself is discarded as "no-target". In the event of detection, the image location is calculated automatically. All stages of the ADLC algorithm are implemented onboard using a Jetson-TX1 computer.

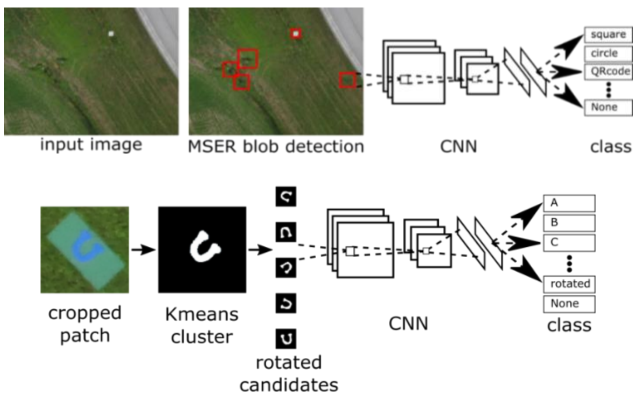

Figure 28. Autonomous detection algorithm

I. Communications and Data Link

- Data Link:
  Three separate subsystems are used for communication between the airplane and the ground station. The subsystems are categorized according to task requirements: autopilot control link (900 MHz) for telemetry and data using RFD-900 radio system, manual control link for the safety-pilot (2.4 GHz) using the FUTABA RF system, and main imagery data link (5.8 GHz). The frequency of 5.8 GHz provides faster image transmission. Moreover, 2.4 GHz is already used for the safety pilot, thus eliminating any chance of interference. The flowchart in Fig 29 shows the data link units and frequencies used.

Figure 29. Communication system flowchart

- Main Imagery Data Link (5.8 GHz):
  Taking last year's approach into consideration, it was decided to stay with the 5.8 GHz band for the main imagery data link. This link is used for online downloading of images during the mission, controlling the on-board camera, and monitoring the OBCs. The considerations included stable work in the presence of the Gr/Ep fuselage, robustness during maneuvers, and broad bandwidth for smooth operation. With regard to transceivers, the UBIQUITI Bullet M5-HP and UBIQUITI NanoStation M5 have proven their effectiveness in the previous years. They fit the required band, have a standard connection compatible with many antenna types, and use the specialized Linux distribution.
- Automated Antenna Tracker:
  This year, it was decided to continue the development of the automatic antenna tracker (AAT) to gain more accuracy and signal strength. The automation allows a crew to avoid RF radiation and low accuracy caused by the manual tracking. Furthermore, it allows to gain another flight line crew member (by eliminating the "human antenna tracker") . Last year, the automated antenna tracker was based on a reverse-engineered MyFlyDream AAT controller. This year, we are developing our own Arduino-based controller. We are planning to develop the following features: determine the orientation of the antenna with GPS and Received Signal Strength Indicator (RSSI) data, wirelessly transmitting the GPS data from Mission Planner to Arduino, and an all-in-one data and power cable with slip ring.
- Antenna Position and Type:
  As in the previous year, this year it was decided to stay with the $\lambda/4$ monopole antenna. It offers a high transmission rate at a relatively long range and would have less interference with the conductive airframe fuselage material than the dipole antenna. In addition, it would receive the ground connection provided by the airframe. The landing gear nevertheless creates interference, and its location

remained stable in the design, thus the antenna location stayed in the rear of the airplane.

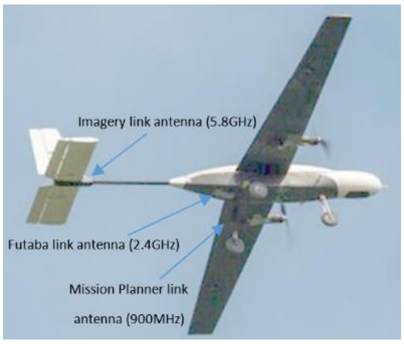

Figure 30. Location of Antennas and Transmitters

- Link Budget:
  We can estimate the receiving power by using the conclusion of the Friis transmission equation.
  According to this theory, the receiving power can be written as:
  $$P_R(\theta_1, \phi_1, \theta_2, \phi_2) = \frac{P_T G_T(\theta_1, \phi_1) G_R(\theta_2, \phi_2)\lambda^2}{(4\pi r)^2} \quad (1)$$
  In analyzing the link budget, we focus on the down link channel. The importance of the transmissions from the plane toward the ground station consist of the imagery data, meaning that:
  - P_R is the power received by the nanostation system.
  - P_T is the power at the bullet output.
  - G_T is the antenna gain.
  - G_R is the nanostation antenna gain.

  Since the camera's USB port has a saturation of 30 Mbps, the entire communication system is affected by it as well.
  However, measurements showed that even with a low P_T value, such as 8 dBm, the received power with 1 km of distance between the plane and the ground station is $P_R \cong -77.7[dBm]$, meaning 48 Mbps. This means the utility of the communication channel at the current condition is not lower than the saturation bound.
- GNSS:
  This year it was decided to tackle the lack of accuracy in geolocation, derived from the GPS.
  These inaccuracies influence our mission in several ways:
  - Geolocation of identified targets, which uses plane location and camera angles.
  - Visual Aided Navigation implements the Simultaneous localization and mapping (SLAM) algorithm.
  - Autonomous landing and take-off uses longitude, latitude, and altitude in order to follow programmed instructions.
  - The air-drop assistance algorithm is based on geolocation.

  After a search for a solution, it was decided to upgrade our GPS to EMLID REACH RTK. The system includes two stations, a base station and a rover station, which correct each other to enable maximum accuracy. The system uses GNSS, GPS, GLONASS, and other systems. The schematic of the location correction is presented in Fig 31.

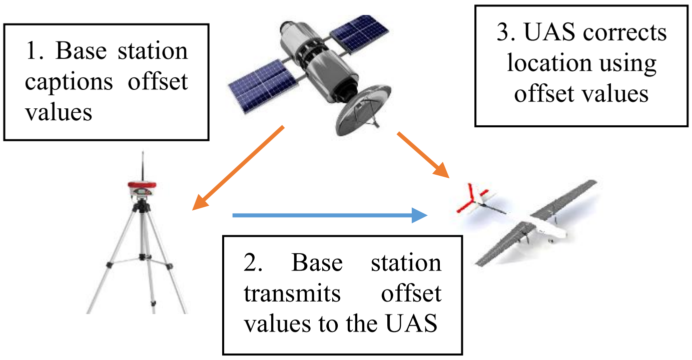

Figure 31. GNSS work visualization

J. Interoperability

The algorithm for the interoperability task, developed by the students, has been integrated into the main loop of the GCS software. It uses the HTTP protocol, which operates on top of the TCP protocol to send and receive information from the server. If the server returns an error, the software sends a message containing the error description and its cause. The process then stops, allowing the system to reconnect to the server. The algorithm comprises HTTP GET and POST requests: login, download obstacle information, off axis target information, emergent target information, and upload UAS telemetry and images. All processes are executed in parallel, using multithreading to allow independent operation.

K. Air Delivery

Three issues were examined: Bottle protection, the release mechanism, and the airdrop algorithm.

- Bottle protection:
  Numerous considerations and experiments were conducted in order to derive the optimal design. Polyurethane foam was chosen for the cushioning material. In addition, attaching the ribbon to the top of the bottle increased the drag and allowed the bottle to land vertically, thus requiring cushioning only at the bottom. Numerous tests have proven the effectiveness of the final design.

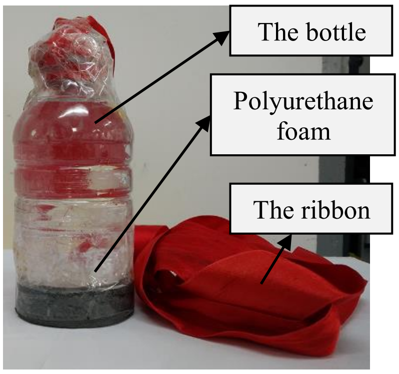

Figure 32. Bottle protection

- Release mechanism:
  The bottle release mechanism has remained identical to the one operated in the previous year's system since it was proven to be effective and sufficient for the needs of the mission. It is based on a 2-door bay. The bay doors remain closed until the servo holding them receives the command.
- Airdrop algorithm:
  The airdrop algorithm continuously calculates the ballistic flight equations in real time. In these equations, it calculates the optimal point of release while taking into consideration full system lag, the real wind profile, and the drag force on the bottle. It was developed in Python and connects to the Mission Planner environment. The process consists of two steps: the measurement and the actuation of the drop. The measurement algorithm calculates the flight path for our platform, in order to position it at the best point for the drop to occur and hit the target. The drop algorithm calculates the drop point itself (the point at which

the servo should command the bay to open) so that the bottle will hit the target (within the acceptable radius).

In the unlikely event the algorithms malfunction, the bottle bay may be opened using the manual control. The point is calculated by a crew member who evaluates the approximate point of release using the visual location of the UAS in the Mission Planner environment and its measured speed and altitude.

L. Autopilot and Flight Control System

For years, the Technion Aerial Systems (TAS) team has been using the 3DR Pixhawk Open Source autopilot platform and its compatible Mission Planner software as its Flight Control System. The system is continually modified and configured for specific SUAS competition tasks. The system has proven itself reliable, well documented, user-friendly and affordable. Our team therefore decided to continue developing this autopilot this year as well, although off-the-shelf alternatives do exist in the market. A compatible open source GCS software application, Mission Planner, was chosen to accompany the overall Autopilot system. It enables implementing all the competition tasks in the environment and performing them, in addition to integrating external Python scripts. Figure 33 illustrates the Mission Planner software during the flight test.

Figure 33. Mission Planner Overview

M. Cyber Security

- <u>Radio Link Protection:</u>
  Radio link protection includes the encryption and the authentication of the link. Ground and airborne stations have encrypted communication using Advanced Encryption Standard (AES). AES is based on a design principle known as a substitution–permutation network (SPN). This combination of substitution and permutation makes communication safe in terms of cybersecurity. Authentication of the users who control the airborne computer is achieved using an SSH connection, a cryptographic network protocol and operation of network services securely over the network, and the WPA2 security protocol in order to secure the WIFI connection.
- <u>Ground Station Protection:</u>
  The communication between the GCS computers is performed via Ethernet and is not detectable. The commands from the station to the antenna tracker are executed

Preprint submitted to 58th Israel Annual Conference on Aerospace Sciences.
Received October 7, 2017.

via wired serial communication, which is safe from cyber threats as well. Access control ensures only authorized personnel have access to the onboard computers (ODROID and Jetson TX1) and the GCS computers. In addition, in order to prevent unrecognized devices from connecting to the network, only specific MAC addresses are allowed to connect. Certainly, to minimize the risk of attack, the network is isolated from external networks, such as the internet, during the mission. However, since full network isolation is not always possible, and as a counter-measure, a firewall is employed. The firewall configured to allow only specifically defined communications needed for system operations.

IV. Test and Evaluation Plan

The mission's success hinges on validation of the expected behavior of all systems and subsystems. The validation required the performance of numerous tests in various fields included in the scope of the project.

N. Developmental Tests

During the construction phase of the UAS, several tests examined the parts which were reconstructed or modified in the current year's design. The results of these tests prove the reliability of the engineering decisions made during the design phase.

7. Wing Loading Test

The wings must withstand the load they will bear continuously during flight. Thus, the wing loading tests are conducted in order to prove the airworthiness of the entire platform. In the scope of this test, the wings are simulated in order to test loading similar to that which is experienced during the flight. The weight is distributed according to the vortex lattice method (VLM) calculation, and the tip deflection is measured. The final results are compared to those calculated using the finite element method analysis.

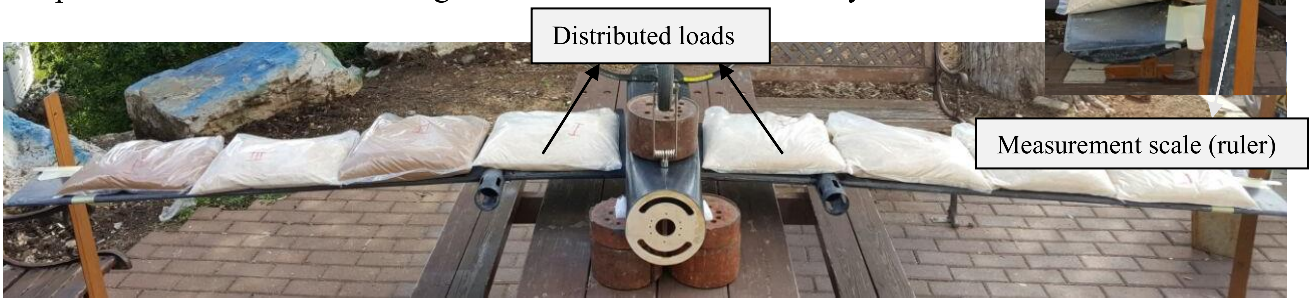

Figure 34. Wing Loading Test

8. Static Thrust Test

A static thrust test was performed in order to validate the expected engine performance, to meet the required UAS flight characteristics. The old and new configurations were compared. The data was calculated using flight mechanics equations and then validated using a static thrust test and eCalc software at our workshop. The common value of T/W ratio for our type of UAV is approximately 0.9; any value above that will provide us with more reserve thrust power in the event of an emergency (such as stalling at low altitude).

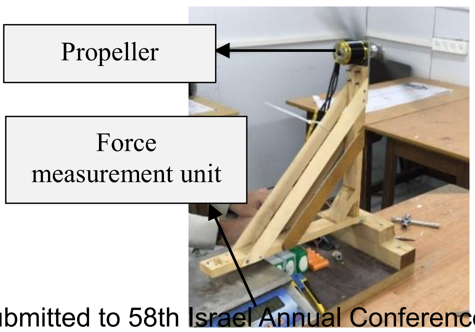

Figure 35. Static Thrust.

Table 4. A comparison between the old and new configuration

	Weight (g)	Prop	Thrust/ Weight	Flight Time (min)	ESC	ESC $	Motor	Motor $	Total for 2 UAV
2016 Configuration	13000	XOAR 17X10	0.63	35	CC Phoenix Edge HV 80	214	Plattenberg 25-16 590KV	250	1856 $
2017 Configuration	12000	APC 18X12	1.46	29	Scorpion Tribunus 120A	85	Scorpion HKIII-4035-560	100	740 $

9. Gimbal Loading Simulation

The gimbal loading simulation was performed on the CAD gimbal model under the loads occurring during the flight. As the results of analysis show, the maximum stress developed in the gimbal structure is approximately 9.5 MPa, which is significantly below the maximum material strength.

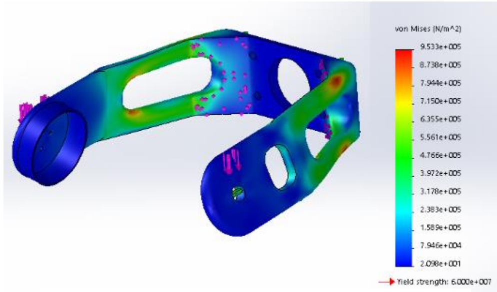

Figure 36. Gimbal loading simulation

10. Wing Loading Simulation

In order to validate the newly designed wing structure’s ability to bear the required stress, finite element analysis (FEA) was performed using the ANSYS software. The results were analyzed to approve continuing with the selected design. Figure 37 illustrates the simulation results.

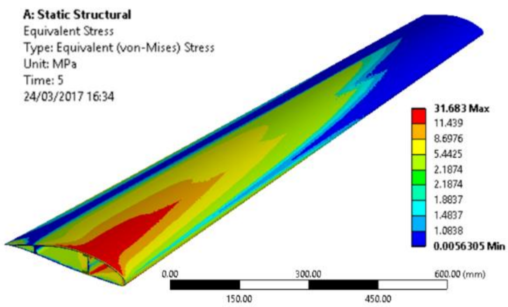

Figure 37. Wing Loading Simulation

11. Wing Structure Composition Experiments

As discussed in the Design section, tests were conducted to derive improvements to the wing skin composition in order to create a lighter and equally or more reliable wing structure. The results of these experiments are presented below. First, the stress and strain diagram performed on four composition options is presented below. It shows explicitly that the thin graphite/epoxy skin with a hard balsa wood core gives the optimal Young modulus in the strain experiment. The 3-point bending experiment results are shown in Fig 38. The overview of the experiments is seen in Fig 39. The hard balsa wood covered with thin Gr/Ep layers skin (marked red in the graphs legend) was chosen for the final design out of several criteria.

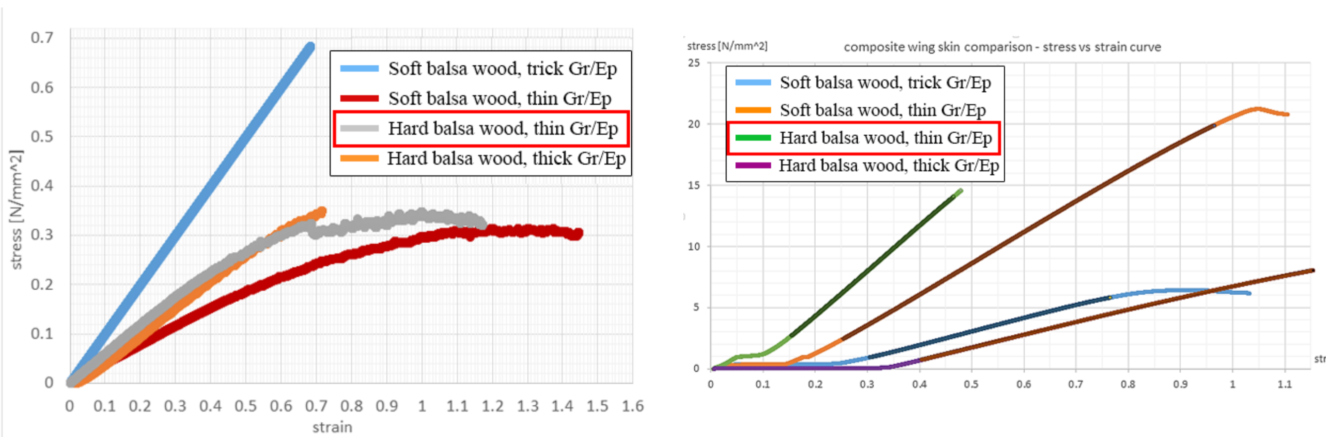

Figure 38. Results of stress and strain experiment (left) and 3-point bending experiment (right)

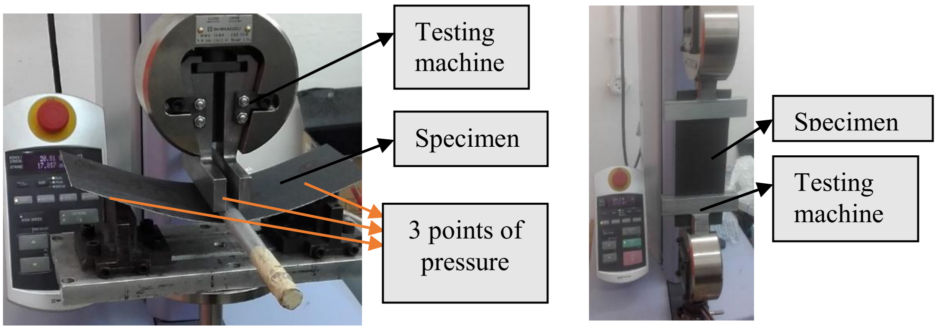

Figure 39. 3- point bending experiment (left); stress and strain experiment (right)

O. Individual Component Testing

A critical phase of the overall design is the component testing, conducted to verify the desired performance of the system in its mission-critical tasks. Testing of the autonomous flight, imaging and object detection, classification and localization, communication, and air delivery are described below.

12. Autonomous Flight

Autonomous flight is one of the fundamental capabilities of an autopilot. This year, the emphasis was put into control loop optimization in order to maximize the performance of the aircraft during the mission.

Numerous flight tests must be conducted to ensure successful performance of the autonomous flight missions. On the missions with the highest risk of failure (e.g., autonomous landing), the testing included a test sequence of three main vehicles in order to minimize risk to the competition air platform.

Each control loop was tuned with specific PID parameters. First, the altitude control loop was tuned until the airplane was able to hold stable, continuous constant altitude. Then, the altitude control was tuned by the reaction of the airplane to manual disturbances given by the safety pilot.

In order to optimize WP navigation, ArduPlanes' L1 navigation control was tuned, allowing the airplane much more accurate and smooth waypoint transition. As illustrated in Fig 40, after the tuning, the aircraft path has become much smoother and less aggressive, with damping close to the critical value.

Furthermore, the Total Energy Control System (TECS) controller was calibrated. The TECS controller calculates the total energy required (both potential and kinetic energy) and pairs it with throttle percentage to calculate the desired energy sum. Testing was executed using loitering flight and constant slope flight, until it reached a reasonable path.

The search area survey grid is dependent on the camera characteristics and the flight envelope, thus deriving altitude (camera resolution), maximal cruising airspeed (shutter frequency), and the optimal line spacing to allow appropriate coverage of the search area; this in turn allows frame overlapping, to minimize the chance of missing the targets. The grid direction can be fit according to the wind direction to minimize disturbances.

In the search area grid, lines were spaced using the every other line" technique, which provides better coverage and allows the aircraft to turn more smoothly.

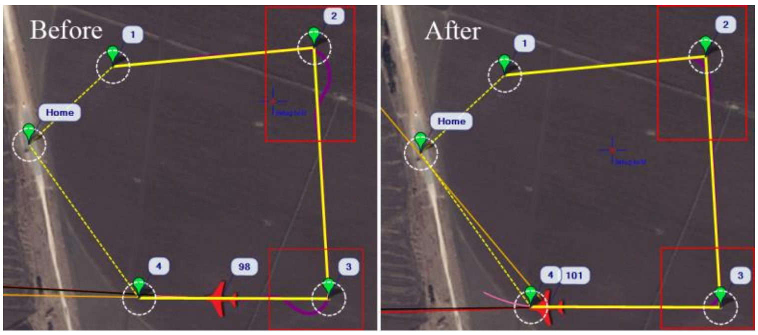

Figure 40. Waypoint following optimization

- <u>Obstacle Avoidance:</u>
  The field tests were performed on the obstacle avoidance algorithm. The environment was brought as close to reality as possible, with a computer simulating a judge's server station, sending the mission details (including the obstacle field) and the GCS calculating the safe trajectory using the algorithm. The following image explicitly shows the UAS trajectory following the new calculated path and avoiding the obstacle presented in its path.

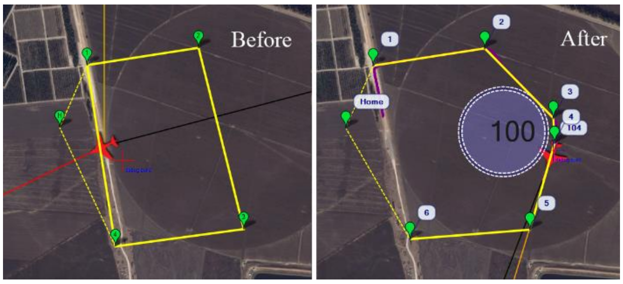

Figure 41. Obstacle Avoidance Demonstration

- <u>Autonomous Takeoff and Landing:</u>
  The main focus this year is to successfully implement autonomous landing, thereby creating a fully operational autonomous air vehicle. As a measure of risk management, the auto-landing software and hardware have been tested with three different platforms. The first test used an off–the-shelf RC airplane, which resembles the 2016 platform and STRIX in terms of dimensions and weight. Next, the previous year's platform was used. Finally, the STRIX system itself performed an autonomous landing, as described in Fig 42. In order to allow safe, accurate touchdown during landing, the Garmin Lidar Lite V3 (Figure 43) was used, providing precise, high-rate altitude measurements. After analysis of the received data, we used the built-in extended Kalman filter (EKF) to better estimate altitude using the multiple sensor input.

Figure 42. Testing Platform Sequence

Figure 43. Garmin Lidar Lite V3

Figure 44 illustrates a typical landing approach, where the waypoints correlate to the waypoint input in GCS.
The landing parameters and log data were recorded and analyzed. The results determined the autonomous landing parameters presented in Table 5. The landing sequence is described in Fig 45.

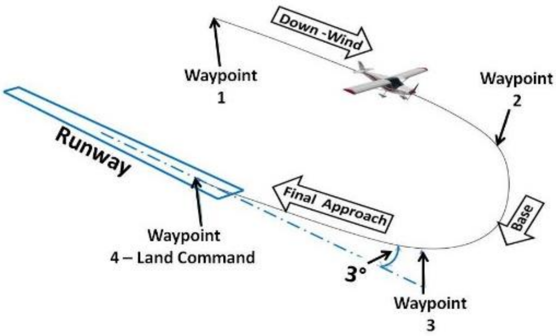

Figure 44. Autonomous Landing Sequence

Table 5. Autonomous Landing Parameters

Parameter	Value	Parameter	Value
Sink Rate	0.25 [m/s]	Glide Slope	2^o
Flare Altitude	0.8 [m]	Max (Pitch Up)	$+6^o$
Flare Timing	2 [s]	Min (Pitch Down)	$+0.85^o$
Approach Speed	12 [m/s]	Throttle @ Final	14 %

Figure 45. Autonomous Landing Sequence Flowchart

The autonomous takeoff is achieved by pointing the airplane along the runway and ensuring there is a steady heading reading. Then the Auto-Takeoff command is sent, and the aircraft is set to maximum throttle percentage. It uses the gyro sensor reading to maintain its heading, and eventually uses GPS when sufficient GPS readings have been made. Pitch is set to a specific value, until target altitude is reached.

13. Imaging and Object Detection/Classification/Localization

A simulation tool was developed in order to validate our imaging code modules. This tool simulates the camera and Pixhawk devices. In this way, we can check specific extreme cases, and compare different neural networks and blob detection algorithms. In addition, this tool has a “live update” option, which displays the output of each detection stage (blob detection, shape classification, and letter classification) on the screen and enables us to test the entire detection process quickly and comfortably. Figure 46 illustrates these stages.

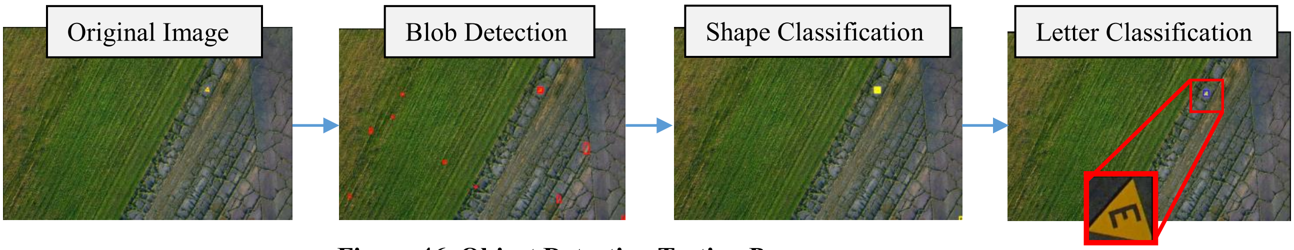

Figure 46. Object Detection Testing Process

14. Air Delivery

The algorithm was tested during the flight first in order to validate the shock absorber used to guarantee safe air delivery. The air-drop algorithm was tested in order to calibrate the drag coefficient and the environmental effects.

15. Communications

In order to test the overall communication between the OBC and GCS, we analyzed two different communication channels: up-link, from the ground station to the plane, and down-link, from the plane to the ground station. Each of the channels has a different transmitting power, which is reflected when calculating the power received at the destination using the Friis formula:

$$Power_{Received}[dB] = Power_{Transmitted}[dB] + Gains[dB] - Losses[dB] \quad (2)$$

Calculating the $P_{Received}$ value for each communication channel using measurements of the parameters above results in:

$$P_{received_{Downlink}}(R)[dBm] \approx -1.71\ [dBm] - 20\log_{10}(R)[dBm]$$

$$P_{received_{Uplink}}(R)[dBm] \approx -3.71\ [dBm] - 20\log_{10}(R)[dBm]$$

Hence, the dependence of the signal intensity (in dBm) in the distance between the transmitter and the receiver is shown in Fig 47.

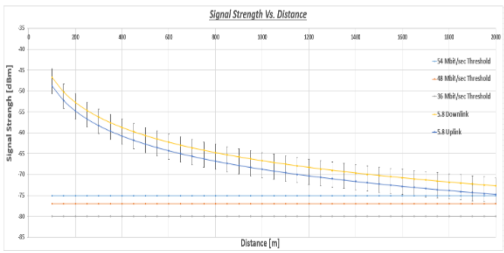

Figure 47. Signal Intensity vs Distance

- <u>Client-Server Communication:</u>
  As part of the communication tests, client-server communication was tested for a visual indication of the bit rate transportation between the antenna and the ground station. During these tests, it was noticed that the bit rate is approximately 10 Mbps, i.e., 34 Mbps under the upper band. This is significantly below expectations. We concluded that use of the incorrect bullets over the past year had damaged transportation performance, so the bit rate using new bullets was analyzed. The result on the client-server communication was approximately 80 Mbps (as displayed), i.e., 30 Mbps, which completely satisfied the requirements.

P. Mission Testing

First, the flight envelope was tested and validated. During the subsequent step, each mission was completed separately. In addition to the simulations and the tests of the specific tasks, full mission tests were conducted. These tests included all the mission tasks performed in the sequence in which they will occur during the competition itself. We held two major mission testing days to run the “GO/NO GO” tests. For these tests, the supervisor was present and evaluated the performance and the mission demonstration of the crew and the UAS. If the requirements were not met during the second test, meaning the crew was not ready to perform the mission, participation in the competition would be cancelled.

The predicted results had to indicate that all mission tasks were performed successfully. Each mission task had a backup plan. If a particular mission task was not fulfilled, the crew had to proceed in performing the sequence of other mission tasks to receive points for the demonstration.

V. Safety Considerations

Table 6. Safety, risks and mitigations considerations

	Risk Factor	Description	Impact	Likelihood	Mitigation Method
Developmental Risks	**Design and/or manufacturing delays**	Delays in developing new flaps, gimbal, pod, system, architecture, and new algorithms may cause delay in the manufacturing process	High	Medium	• Kicking off the development process before the academic year in order to meet the schedule • Determine deadlines for development to use old system components and algorithms • Perform the design review (PDR, CDR)
	Manufacturing mistakes and structure failures	During manufacturing and the building process, there is a high probability of discrepancies between components; this may lead to structure failure	High	Low	• Create a complete, detailed design with sufficient tolerance for manufacturing discrepancies • Consulting experts in manufacturing with composite materials • Testing structure for maximum load • Using safety factors
	Integration issues	Since the system was developed by students from two faculties (Aeronautics and Electrical Engineering), there may be contradictory requirements and solutions that may endanger integration of the subsystems. Effective cooperation between the two faculties is essential. In addition, integration of new components in the system may result in risk and delays in development.	Medium	Medium	• Weekly design review meetings were conducted with participants from both faculties • A single faculty advisor led the combined team

Preprint submitted to 58th Israel Annual Conference on Aerospace Sciences.
Received October 7, 2017.

Mission Risks	**Breach of competition's rules**	The competition includes highly detailed rules, and the system must comply with all of them	High	Low	• One team member was assigned to be in charge of addressing any legal issues and system safety • A thorough inspection of the rules and regulations was made before airframe design
	Crash during autonomous landing practice	Execution of autonomous landing required preliminary training, which included the landing itself; this could result in a crash	High	Medium	• Divide autonomous landing practice among three different platforms: ○ A dedicated trainer ○ Last year's UAS ○ STRIX • Following the flight instructions and the checklists
	Insufficient crew training	Schedule delays might result in insufficient flight time, affecting both debugging the system performance and training the team	Medium	High	• Using the Mission Planner Simulator for flight operator training • Initial team training was done using last year's system and a training plane
Operational Risks	**Crash during testing**	Air vehicle crash during evaluation and system flight tests may endanger the team's ability to participate in the competition	High	Medium	• The 2016 aircraft is maintained as a backup solution for training • Building two identical STRIX platforms
	Bottle release	The bottle may be released in the presence of unexpected winds and gusts, which may endanger crew members	Medium	Low	• Setting airdrop position far from the ground station and crew members • Revision of the air delivery process while still on the ground

VI. Conclusions

The STRIX system is designed, built, and integrated to meet the AUVSI 2017 competition requirements and to give the best performance while performing the mission tasks. During the year, the team performed all the scheduled engineering processes, which included initial requirements analysis, implementation of a "red team" approach to carefully evaluated the previous system design , making the final design decisions, the manufacturing process, and tests and evaluation of the system and subsystems. Numerous flight hours were accumulated during flight tests, which occurred every week for the duration of the project. This experience has advanced the system and the crew in their readiness for the competition tasks and the overall mission.

Finally, the team underwent an intensive learning process while completing the project tasks. Experience was gained not only from an engineering perspective, but also from the project management process, from its initial design stages and requirements analysis to the final mission evaluations and tests.